Connecting the global H-mode power threshold to the local radial electric field at ASDEX Upgrade

M. Cavedon[1], G. Birkenmeier[1], T. Pütterich[1], F. Ryter[1], E. Viezzer[2], E. Wolfrum[1], R. Dux[1], T. Happel[1], P. Hennequin[3], U. Plank[1], U. Stroth[1,4], M. Willensdorfer[1] and the ASDEX Upgrade Team‡

[1]Max-Plank-Institut für Plasmaphysik, D-85748, Garching, Germany
[2]Dept. of Atomic, Molecular and Nuclear Physics, University of Seville, Avda. Reina Mercedes, 41012 Seville, Spain
[3] Laboratoire de Physique et Technologie des Plasmas, Ecole Polytechnique, 91 128 Palaiseau, France
[4]Physik-Department E28, Technische Universität München, 85748 Garching, Germany

11 March 2020

Abstract.

The relation between the macroscopic input power required at ASDEX Upgrade to access the H-mode P_{thr} and the microscopic $\mathbf{E}\times\mathbf{B}$ shear has been investigated via fast charge-exchange recombination spectroscopy (CXRS) measurements at various toroidal magnetic fields, different electron densities, and in both hydrogen and deuterium plasmas. For the H-mode onset, a threshold in the $v_{\mathrm{E}\times\mathrm{B}}$ minimum, an approximation of the $\mathbf{E}\times\mathbf{B}$ shear, has been found. This identifies $v_{\mathrm{E}\times\mathrm{B}}$ and not E_r as the important player for the L-H transition. A database of measurements including CXRS, Doppler reflectometry measurements and comparison to neoclassical approximations shows a threshold $v_{\mathrm{E}\times\mathrm{B}}$ of $(6.7 \pm 1.0)\,\mathrm{km/s}$ ranging over a factor of three in P_{thr}. Using these findings, a simple derivation of the P_{thr} scaling is proposed giving a physics interpretation of the B_t, density and surface dependence of P_{thr}.

Submitted to: *Nucl. Fusion*

1. Introduction

It is widely accepted that the $\mathbf{E}\times\mathbf{B}$ velocity shear, caused by the local radial electric field E_r, is responsible for the suppression of turbulence and therefore for the establishment of the edge transport barrier (ETB) which is the characteristic feature of the H-mode [1]. The formation of the ETB coincides with the transition from the low (L-) to the high

‡ See author list of H. Meyer et al. 2019 Nucl. Fusion 59 112014

confinement mode (H-mode) and is triggered when the heating power exceeds a certain threshold $P_{\rm thr}$, which has the following inter-machine scaling [2]:

$$P_{\rm thr,scal08} = 0.049\, n_e^{0.72}\, B_t^{0.80}\, S^{0.94}. \quad (1)$$

The scaling gives the required power in MW for a given line averaged density n_e in $10^{20}\,\mathrm{m}^{-3}$, magnetic field B_t in T and the plasma surface S in m^2. Note that $P_{\rm thr,scal08}$ does not scale linearly with n_e [3, and references therein] and only the monotonic part at high densities (high density branch) is considered in the regression (1). Below a certain electron density $n_{e,\rm min}$, the L-H power threshold is observed to increase with decreasing density (low density branch). A possible explanation for this behaviour is reduced collisional energy transfer from electrons to ions at low densities [4, 5]. Power balance analysis of ASDEX Upgrade (AUG) and Alcator C-mod discharges showed a linear dependence of the edge ion heat flux at the L-H transition $Q^{\rm LH}_{i,\rm edge}$ on density [4, 6, 7]. In particular, in the low density branch, electrons are usually heated directly while ions are weakly coupled to the electrons, resulting in an increase of $P_{\rm thr}$. The edge ion heat flux defines the local ion temperature and pressure gradient and, in turn, the equilibrium radial electric field $E_{r,\rm neo}$ which is approximately opposite to the main ion diamagnetic flow velocity $v^i_{\rm dia} = \nabla p_i/(Z_i n_i B)$ where n_i, p_i and Z_i are the main ion density, pressure and charge, respectively [8]. In line with this, at ASDEX Upgrade, a constant minimum E_r value, which can be used as an approximation of ∇E_r, has been found at the L-H transition independent of the electron density, suggesting that a certain value of $E_{r,neo}$, and the related flow shear, is required to access H-mode [9]. Note that the neoclassical component of the radial electric field has been found to be the dominant contribution to E_r in H-mode [10, 11], while close to the L-H transition it is still disputed since other contributions, e.g. zonal flows or ion orbit losses, are reported to be important [12, 13, 14, 15, 16]. Still, the equilibrium (neoclassical) $v_{\rm E\times B}$ is in most of the L-H transition theories responsible for locking into the H-mode [12].

In this work, the correlation between the E_r profile just before the confinement transition and $P_{\rm thr}$ is investigated in order to experimentally relate the global effects of input power and e-i heat exchange to the local $\mathbf{E}\times\mathbf{B}$ velocity shearing of turbulence. In particular, the minimum of the E_r well, used as proxy of ∇E_r [17], just before the L-H transition is measured extending the database in [9, 18] to different L-H power threshold values obtained via a variation of magnetic field, density and isotope mass (deuterium and hydrogen) (Section 3). To this purpose, a detailed characterization of the L-H transition dynamics is reported in Section 2 to consistently define the L-H transition time points. Finally, based on these results, a possible physics interpretation of the power threshold scaling (1) is given (Section 4). Summary and conclusions can be found in Section 5.

2. Experimental setup

In order to make a link between the $\mathbf{E}\times\mathbf{B}$ velocity shear and the H-mode onset, it is necessary to define a time point where the plasma changes its confinement state thus

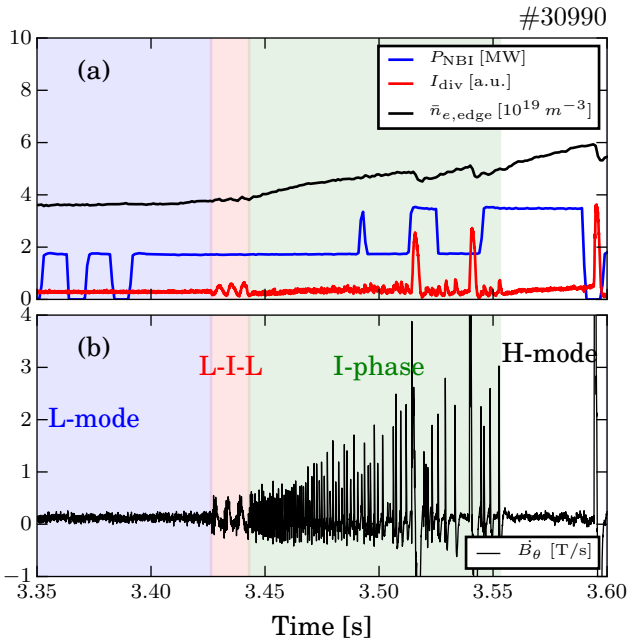

Figure 1: Evolution of a typical L-H transition at AUG considered in this work. (a): NBI power (blue), integrated edge electron density (black) and divertor shunt current (red), (b): Poloidal magnetic field fluctuation measured close to the secondary X-point.

enabling a comparison of different discharges. A dedicated series of eight discharges has been performed in which several L-H transitions (24 in total) have been induced by slowly ramping the input power up via neutral beam injection (NBI). NBI allows for charge exchange recombination spectroscopy measurements. In particular, the fast edge CXRS [19] in combination with helium seeding has been employed to have good statistics also within short NBI blips. The plasma current has been kept constant at 0.8 MA due to the dependence of P_{thr} on I_p at low densities [20] inducing a variation of q_{95} between 3.6 and 6.3. Feed-forward deuterium gas puff of 10^{21} particles/s with constant divertor pumping has been employed resulting in slightly different n_e. Figure 1 shows the time evolution of a typical L-H transition analysed in this work. The time traces of input power P_{NBI} (blue), line averaged edge electron density $\bar{n}_{e,\mathrm{edge}}$ and the divertor current I_{div} (red) are reported in figure 1(a) while the poloidal magnetic field fluctuation $\dot{B}_\theta$ measured by a Mirnov-coil located close to the secondary X-point is shown in figure 1(b). The latter signal is used to characterize the evolution from L-mode (highlighted in blue in figure 1) to a fully developed H-mode during which, at AUG, the plasma goes through an I-phase [21, 22] (green in figure 1) often preceded by a L-I-L dithering phase (red in figure 1).

The L-I-L dithers can be confused with divertor oscillations, i.e. the oscillations between detached and not-detached divertor states [24]. As discussed in [25], both oscillatory phenomena take place in medium to high density L-modes close to the L-H transition and show similar behaviour in the divertor shunt currents (figures 2(a) and (b)), in the edge density (figures 2(c) and (d)) and in the inner (red) and outer

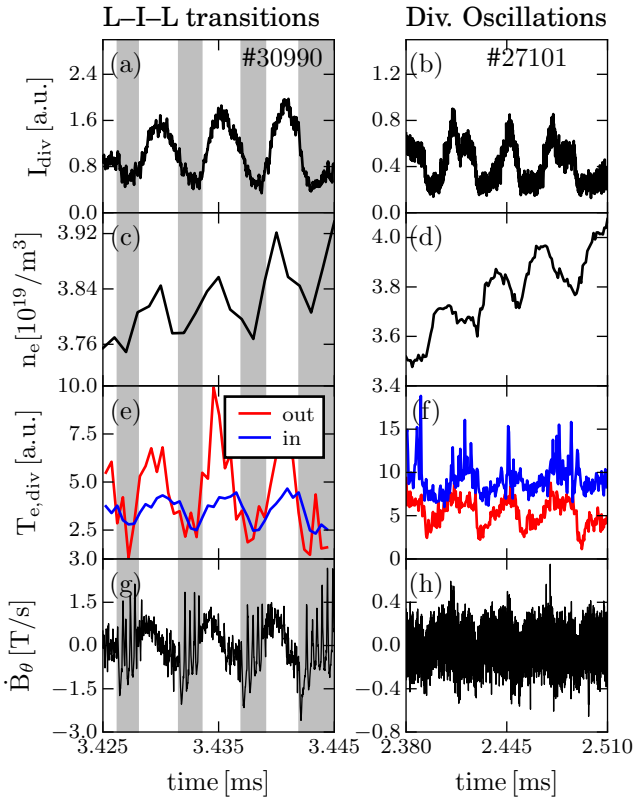

Figure 2: Comparison between L-I-L dithers (left-hand side) and divertor oscillations (right-hand side). (a)-(b) divertor shunt current, (c)-(d) edge electron density, (e)-(f) inner (blue) and outer (red) target temperatures, (g)-(h) poloidal magnetic fluctuations. The divertor oscillations are taken from a discharge published in [23].

(blue) target temperatures (figures 2(e) and (f)). However, the L-I-L dithers exhibit the typical bursts in $\dot{B}_\theta$ during the I-phase part (figure 2(g), highlighted in gray) which are not present in the divertor oscillations (figure 2(h)). Furthermore the frequency of the L-I-L dithers is usually higher compared to the frequency of the divertor oscillations.

The onset of the I-phase is associated with a clear confinement improvement seen in the edge density and in the appearance of type-I ELMs (figure 1, $t \approx 3.52, 3.54\,\mathrm{s}$). Moreover, as reported in [16], a rapid change in the edge gradients and in E_r is observed once entering the I-phase. Hence, to analyze the background condition for the H-mode confinement change, the $\mathbf{E}\times\mathbf{B}$ shear needs to be analyzed before the L-I transition. Following the same logic, within the L-I-L dithers, only time points during the short L-mode phases are considered. These time points in the evolution from L- to H-mode will be simply referred to as L-H transitions in the following. In order to resolve these short time windows and, at the same time, obtain a good signal to noise level, a time resolution of 100 µs to 200 µs has been employed. Figure 3 compares the evolution of the maximum of the $v_{\mathrm{E}\times\mathrm{B}}$ velocity with a time resolution of 100 µs (fig. 3(a)), the input power (fig. 3(b), red) and $\dot{B}_\theta$ (fig. 3(b), black) across an L-I transition without any L-I-L dither. Note that at AUG, CXRS measurements are only possible if the NBI is

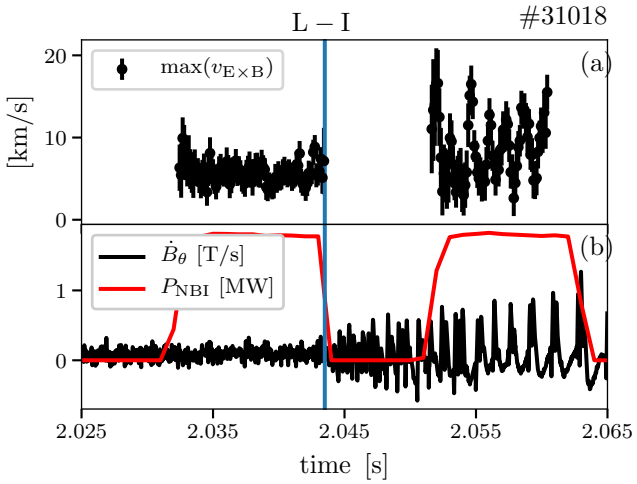

Figure 3: L-I transition triggered by an NBI blip. (a): max $v_{E\times B}$, (b) NBI input power (red) and $\dot{B}_\theta$.

switched on. As in many of the investigated discharges, the L-I transition is triggered during or right after an NBI beam blip, which is typically 12 ms to 20 ms long. In the corresponding L-mode phase, the maximum of the $v_{\mathrm{E\times B}}$ velocity is rather constant and hence, to improve the signal to noise ratio, the last ten L-mode spectra has been averaged. The resulting time resolution is in between 1 ms and 2 ms which is enough to study the background condition for the L-H transition, consistently with the aim of this work. Due to the low integration time, the same approach could be used also for the evaluation of L-I-L in which, moreover, many L-I transitions could be averaged together.

3. E_r minimum at the L-H transition

In this section, the E_r minimum, a proxy of the E_r shear [17], is shown at the L-H transition in discharges with different values of n_e, B_t, and the plasma isotope. Other P_{thr} dependencies, not included in the scaling (1), have been kept constant to decouple them from the plasma parameters of interest. All other plasma parameters have been kept constant including the one important for divertor conditions e.g. plasma shape, strike point position. Therefore, it is expected that the radial electric field in the Scrape Off Layer (SOL) stays constant since it is roughly equal to $E_{r,\mathrm{SOL}} \approx 3e\nabla T_{e,\mathrm{target}}$ [26]. In this way, the minimum of E_r can be taken as a proxy of both the outer and the inner shear layers which can both trigger the L-H transition [27]. Furthermore, the choice of taking the E_r minimum instead of the inner or outer gradient themselves is also due to the limited amount of radial lines-of-sight which can be acquired with the fast CX system, i.e. five poloidal and four toroidal positions, making the estimation of both gradients at the same time highly uncertain.

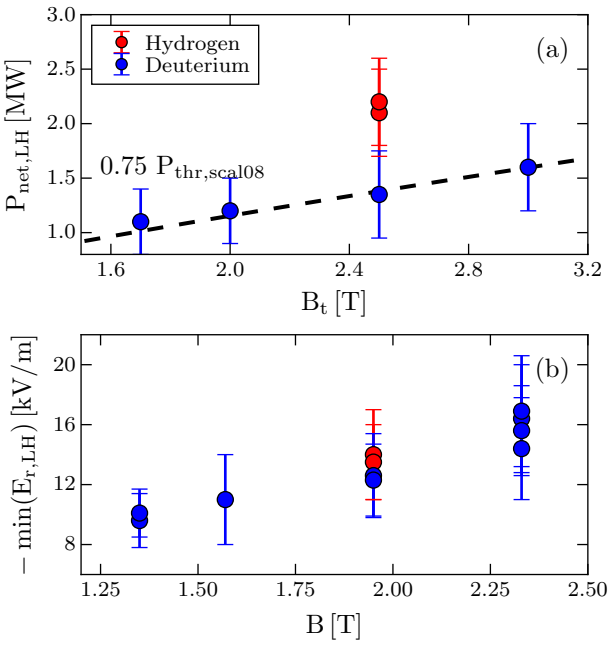

Figure 4: (a) L-H power threshold as a function of the toroidal magnetic field, (b) E_r minimum as a function of the local magnetic field at the measurement point. Discharges in hydrogen are shown in red and deuterium in blue. The dashed line in (a) indicates the power threshold scaling from [2] rescaled by 0.75 following the metal wall effect [20].

3.1. Toroidal magnetic field scan

The almost linear dependence of the L-H transition power threshold on the toroidal magnetic field B_t (see equation (1)) is not very well understood as of yet. However, the dependence of the power threshold on B_t is very robust as it is observed in every device independently of plasma conditions [2]. In figure 4, the power threshold (4(a)) and the E_r minimum at the L-H transition (4(b)) are shown as a function of B_t. Red points indicate discharges in hydrogen while the blue ones in deuterium. As expected, the power threshold increases with B_t and it is roughly a factor of 1.8 higher in hydrogen plasmas (figure 4(a)). The dashed black line shows the predicted value of the threshold power from the scaling (1) rescaled by 0.75 following the metal wall effect [20]. P_{thr} is calculated consistently to [20], i.e. accounting for the time derivative of the stored energy without subtracting the radiative core losses. Figure 4(b) shows that the absolute value of the E_r minimum just before the L-H transition scales roughly linearly with B. In other words, a constant $v_{\mathrm{E\times B}} = E_r/B$ shear is found at the L-H transition as reported in [28, 25] where, however, only the neoclassical approximation of E_r is shown. In particular, given the effect of the divertor configuration on the SOL E_r [27], the results shown here are consistent with a different E_r minimum for different divertor configurations. Moreover, despite a factor of two in P_{thr}, the hydrogen data align well with the deuterium measurements. Note that the $v_{\mathrm{E\times B}}$ minimum is a proxy of the $\mathbf{E}\times\mathbf{B}$ shear only if the width of the E_r well is constant. This has been shown in [17] for different parameters as

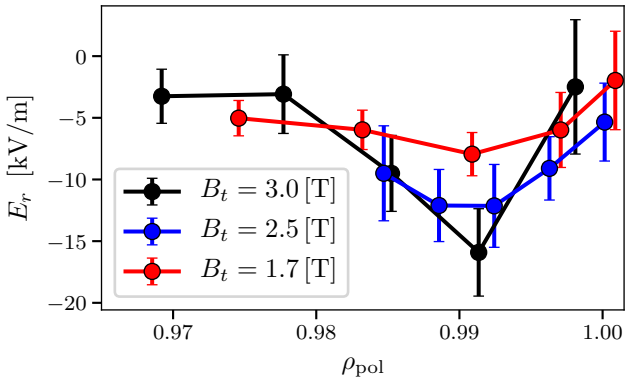

Figure 5: Edge E_r profiles at different magnetic fields before three single L-H transitions.

the confinement regime or the plasma density but for a constant B_t. However, as shown in [29], the width of the pedestal pressure in real space is roughly constant and hence the approximation $\min v_{E\times B} \sim \gamma_{E\times B}$ might also hold for different magnetic fields.

Figure 5 shows three edge E_r profiles obtained at different magnetic field. The radial electric field is evaluated at the position of the He^{2+} poloidal velocity measurements which, multiplied by the toroidal magnetic field, makes the larget contributions in the radial force balance for He^{2+}: $E_r = \nabla(T_i n_{He^{2+}})/(2n_{He^{2+}}) - v_{\mathrm{pol},He^{2+}} B_{\mathrm{tor}} + v_{\mathrm{tor},He^{2+}} B_{\mathrm{pol}}$. The E_r evaluations in this work include all the previous terms. Note that the range between $\rho_{\mathrm{pol}} = 0.97$ and $\rho_{\mathrm{pol}} = 1.00$ corresponds to about 2.0 cm in real space at AUG and that different radial separation of the measurement points is due to the choice of channels for the fast CX spectrometer. During every discharge, the plasma has been anyway radially scanned in between L-H transition to properly resolve the minimum.

These findings may indicate that a critical $v_{E\times B}$ shear is required to access the H-mode. In a simplified picture, the $\mathbf{E}\times\mathbf{B}$ shear ($\gamma_{E\times B}$) needs to overcome an effective turbulence growth rate (γ_{turb}) to induce turbulence reduction and γ_{turb} itself might depend on B_t or the isotope mass. This is for example the case in the gyro-Bohm limit. On the other hand, in a simple linear ion temperature gradient turbulence model, neglecting Laundau damping and finite Larmor radius effects, $\gamma_{\mathrm{turb}} \approx k_\theta \rho_i \cdot v_{\mathrm{th}}/R \cdot \sqrt{L_{T_i}/R}$ where k_θ is the poloidal wave number, ρ_i the ion Larmor radius, v_{th} the thermal velocity, and R/L_{T_i} the normalized ion temperature gradient [30, 31]. This expression depends on B_t via ρ_i. However, due to finite Larmor radius effects, γ_{turb} is zero at $k_\theta \rho_i = 1$ and has a maximum around 0.3-0.5 in linear calculations. On the same line, in non-linear calculations, γ_{turb} has always his maximum around $(k_\theta \rho_i) \approx 0.15$-0.2, making γ_{turb} independent of B_t [32, 33]. Note that both works consider not only ITG but more generally L-mode pedestals and show self-similar spectra. In this way, the turbulence stabilization criteria $\gamma_{E\times B} > \gamma_{\mathrm{turb}}$ is consistently independent on the magnetic field on either sides. However, following this logic, a residual dependence on the mass M as $1/\sqrt{M}$ remains due to the v_{th}-term. Experimental characterization of the turbulence characteristics before the L-H transition for different plasma parameters are unfortunately very scarce. At AUG, a comparison of the turbulence radial correlation

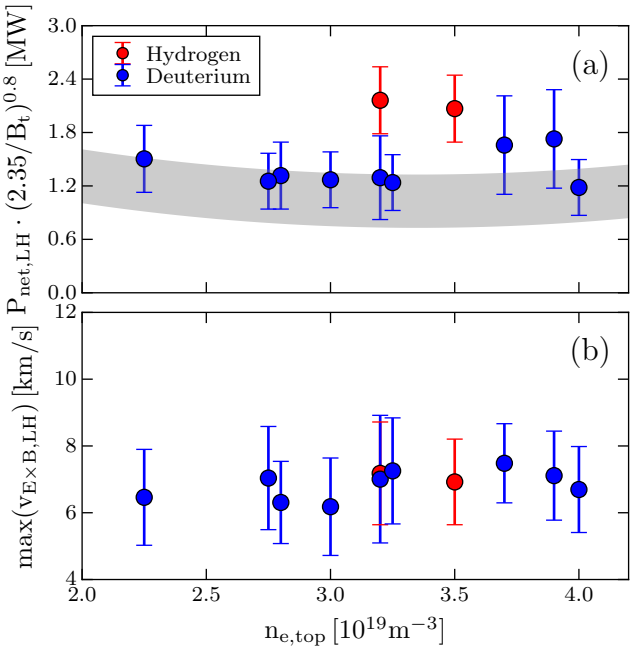

Figure 6: L-H power threshold normalized to 2.35 T (a) and maximum of $v_{\mathrm{E\times B}}$ as a function of the pedestal top density in hydrogen (red) and deuterium (blue) plasmas. The gray band in (a) indicates the measured P_{thr} for AUG as reported in [20].

length in L-mode is shown in [34] in which comparable values in hydrogen and deuterium L-modes are found at the plasma edge. This suggests that the edge turbulence is similar and hence an analogous $\gamma_{E\times B}$ might be required to obtain suppression.

3.2. Electron density scan

This section presents an extension of the findings published in [9]. The dependence of the L-H power threshold on the electron density is not monotonic. In case of ASDEX Upgrade, P_{thr} has a minimum at an electron density of roughly $n_e = 4 \times 10^{19}\,\mathrm{m}^{-3}$. Although it has been found in many tokamaks [28, 35, 36], this feature is not included in the power threshold scaling. In figure 6(b) the minimum of the $\mathbf{E}\times\mathbf{B}$ velocity at the L-H transition is shown as a function of the pedestal top electron density $n_{e,\mathrm{top}}$ for the discharges presented in the previous section. The corresponding calculated power threshold normalized to $B_t = 2.35\,\mathrm{T}$ is shown in figure 6(a) in comparison with the estimation from [20] which is depicted by the grey band. Here, the discharges performed in deuterium plasmas are indicated in blue while the ones in hydrogen are marked in red. The minimum of the $\mathbf{E}\times\mathbf{B}$ velocity at the L-H transition is found to be constant independent of the electron density, similar to the observations in [9] in which the neoclassical approximation has been used.

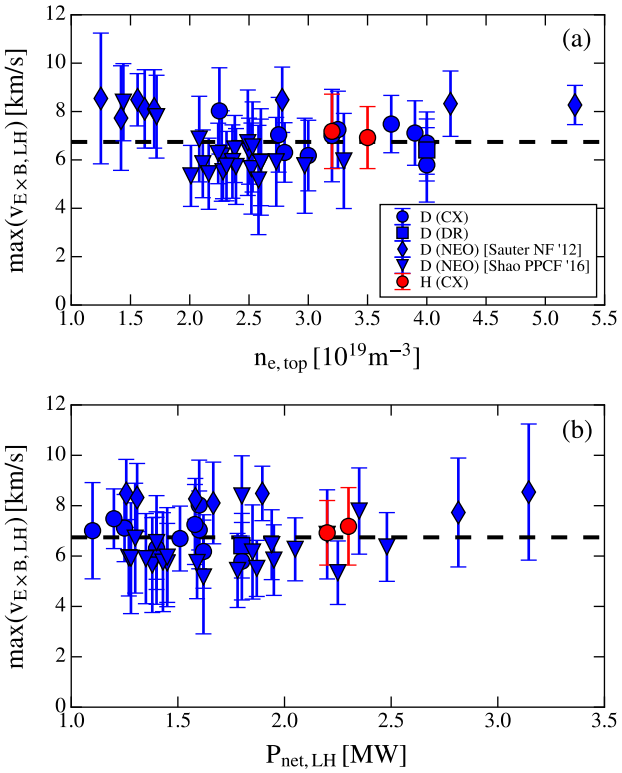

Figure 7: Maximum of $v_{\mathrm{E\times B}}$ as a function of the pedestal top electron density (a) and of the net input power (b). The figures compare data from CX, DR and from [9] and [18] (different symbols) while the different colors (red: hydrogen, blue: deuterium) indicate the different plasma isotope.

3.3. Comparison to previous publications

The findings presented in this section link the $\mathbf{E}\times\mathbf{B}$ velocity to the net input power close to the L-H transition exploring the main dependencies of the L-H power threshold, i.e. B_t and n_e. A threshold in $v_{\mathrm{E\times B}}$ for the L-H transition is found consistently with previous studies at AUG [9, 18]. Figure 7(a) presents a comparison between the measurements of the minimum of $v_{\mathrm{E\times B}}$ discussed in the previous section and the neoclassical estimation published in [9, 18] as a function of the pedestal top electron density. Within the error bars a constant $\mathbf{E}\times\mathbf{B}$ velocity is found over a large range of electron densities, for different B_t values and with carbon and tungsten wall [18]. At the L-H transition the $\mathbf{E}\times\mathbf{B}$ velocity is on average $v_{\mathrm{LH}} = (6.7 \pm 1.0)\,\mathrm{km/s}$. Measurements from CXRS and Doppler reflectometry are compared with the predictions from neoclassical theory showing good agreement within the error bars [9, 18]. This suggests that the background condition of the $\mathbf{E}\times\mathbf{B}$ velocity just before the L-H transition is dominated by the neoclassical $\mathbf{E}\times\mathbf{B}$ velocity. This however does not exclude a contribution from zonal flows to the total $v_{\mathrm{E\times B}}$ on fast timescales and/or that a ZF is a trigger of the L-H transition. The same data of $v_{\mathrm{E\times B}}$ are shown in figure 7(b) as a function of the net input power at the L-H transition. The figure highlights that within roughly a factor of

three of P_{thr}, a certain minimum of $v_{\mathrm{E\times B}}$ is required to access H-mode.

4. Consideration on P_{thr} (only high density branch)

Based on the experimental evidence presented in the previous section and together with previous publications, the scaling of the L-H transition power threshold (1) can be derived based on a few assumptions which are highlighted below:

- the largest contribution to E_r comes from the ambipolar neoclassical radial electric field, i.e. $E_r \approx \nabla(T_i n_i)/(eZ_i n_i)$
- the $v_{\mathrm{E\times B}}$ minimum at the L-H transition is about constant, $\min v_{E\times B,\mathrm{LH}} \approx 6.7\,\mathrm{km/s}$

while the assumptions are:

(i) $T_i = T_e$ such that:

$$P_{\mathrm{thr}} = n\chi_{\mathrm{edge}}\nabla T_i S \tag{2}$$

where χ_{edge} is the heat diffusivity at the edge.

(ii) $eE_r \approx \nabla T_i + T_i\nabla n_e/n_e \approx 2\nabla T_i$. This is in general not valid but both contributions ∇T_i and $T_i\nabla n_e/n_e$ are usually of the same order of magnitude.

(iii) $\chi_{\mathrm{edge}} = 1\,\mathrm{m}^2/\mathrm{s}$.

In this way we can re-write (2) as:

$$P_{\mathrm{thr}} = n\chi_{\mathrm{edge}}\frac{1}{2}\min v_{E\times B,\mathrm{LH}} BS \tag{3}$$

$$\approx 0.05 \cdot nBS \tag{4}$$

with P_{thr} in MW and n, B and S in the same units as in (1). The result well describes both the trends and the pre-factor of the scaling (1) giving a zero order understanding of it: to access H-mode a critical ion heat flux per particle, i.e. $P/(nS)$, needs to be reached to drive enough $E_{\mathrm{r,neo}}$. The critical $P/(nS)$ scales with B since the actual turbulence shearing is done by the $\mathbf{E}\times\mathbf{B}$ velocity. Note that the value of χ_{edge} (assumption (iii)) is ad-hoc to get the right pre-factor in (4) but definitely in the right ballpark while assumption (ii) masks the importance of the n_e profile as reported for instance in [18]. In particular changes in the n_e (n_i) profiles are possibly linked with pumping, plasma shape in the divertor region, divertor geometry itself or changes in the SOL and, in turn, can strongly influence the diamagnetic contribution to $v_{\mathrm{E\times B}}$. Formula (3) proposed in this work is in many aspects similar to the one proposed by Wagner [37] and reported by Connor and Wilson [38] (equation (1.2)) in which, however, an ad-hoc fitting parameter is introduced. Due to the measurements presented in section 2, this is not required anymore. The same approach was also used by Rozhansky at al. [39, 40] in which, using the assumption of a fixed $\gamma_{E\times B}$ at the L-H transition, the scaling (1) could be derived by fitting $\gamma_{E\times B}$ and using a constant χ_i in B2-SOLPS5.0 simulations.

This simple considerations do not aim to unify all the different experimental observations characterizing the transition from L- to H-mode. Many of them require

a deeper knowledge of the influence of the SOL or of the turbulence-flow interaction. Here, only the dependencies of the L-H power threshold reflected in the Martin scaling are considered. A more complete heuristic model based on these principles but also including the low density branch has been recently proposed in [41]

5. Summary and outlook

The dynamics of the L- to H-mode transition has been characterized to identify the strongest confinement change. Just before this time point, the minimum of the $\mathbf{E}\times\mathbf{B}$ velocity, a proxy of the shear flow, is found to be independent on magnetic field and plasma isotopes highlighting the importance of reaching a constant $v_{\mathrm{E}\times\mathrm{B}}$ rather than E_r to trigger an L-H transition, similar to JET results [28, 25]. These findings extend the work done in [9, 18] in which the effect of density and wall material were examined and includes direct measurements of the E_r profile. The analysis of the whole database reveals a constant $\mathbf{E}\times\mathbf{B}$ velocity minimum of $\min v_{\mathrm{E}\times\mathrm{B,LH}} = (6.7 \pm 1.0)\,\mathrm{km/s}$ over a factor of three in the power threshold. Data from CXRS and DR for $\mathbf{E}\times\mathbf{B}$ flow are compared to the neoclassical approximation showing good agreement and indicating that $v_{\mathrm{E}\times\mathrm{B}}$ cancels the ion diamagnetic flow at AUG. Based on these results, a physics-based derivation of the $P_{\mathrm{thr,08}}$ scaling could be obtained by assuming $E_r \approx 2\nabla T_i$ and $\chi_{\mathrm{edge}} = 1\,\mathrm{m/s^2}$. In this picture, $P_{\mathrm{thr,08}}$ is simply the heat flux per particle required to reach a certain $v_{\mathrm{E}\times\mathrm{B}}$. The derivation resembles the one of Wagner [37] and Rozhansky at al. [39, 40] however, does not require any additional fitting parameter.

A direct extension of this work would be the investigation of the effect of the SOL and divertor conditions on P_{thr} and hence on the role of the inner vs outer $\mathbf{E}\times\mathbf{B}$ shear layer. To this extent, a new SOL spectroscopy diagnostic has been installed at AUG. Furthermore a characterization of the turbulence characteristics before the L-H transition from an experimental and theoretical point of view is foreseen. Finally, the simple considerations introduced in section 4 are investigated within a transport code in order to go beyond of the assumptions used here. In this way, a more reliable prediction of P_{thr} might be possible.

Acknowledgments

The author would like to thank C. Angioni, R. Bilato and G. Conway for fruitful discussions and valuable input.

This work has been carried out within the framework of the EUROfusion Consortium and has received funding from the Euratom research and training programme 2014-2018 and 2019-2020 under grant agreement No 633053. The views and opinions expressed herein do not necessarily reflect those of the European Commission.

References

[1] H. Biglari et al. *Phys. Fluids B: Plasma Phys.*, 2(1):1, 1990.

[2] Y R Martin et al. *Journal of Physics: Conference Series*, 123:012033, 2008.

[3] F. Ryter et al. *Nucl. Fusion*, 36(9):1217, 1996.

[4] F. Ryter et al. *Nucl. Fusion*, 54(8):083003, 2014.

[5] M. A. Malkov et al. *Phys. Plasmas*, 22(3), 2015.

[6] F. Ryter et al. *Plasma Phys. Control. Fusion*, 58(1):014007, 2016.

[7] M. Schmidtmayr et al. *Nucl. Fusion*, 58(5):056003, 2018.

[8] F. L. Hinton et al. *Rev. Mod. Phys.*, 48:239–308, 2, 1976.

[9] P. Sauter et al. *Nucl. Fusion*, 52(1):012001, 2012.

[10] R. M. McDermott et al. *Phys. Plasmas*, 16(5), 2009.

[11] E. Viezzer et al. *Nucl. Fusion*, 54(1):012003, 2014.

[12] L. Schmitz et al. *Phys. Rev. Lett.*, 108(15):155002, 2012.

[13] P. Manz et al. *Phys. Plasmas (1994-present)*, 19(7), 2012.

[14] C. S. Chang et al. *Phys. Rev. Lett.*, 118:175001, 17, 2017.

[15] T. Kobayashi et al. *Nucl. Fusion*, 55(6):063009, 2015.

[16] M. Cavedon et al. *Nucl. Fusion*, 57(1):014002, 2016.

[17] E. Viezzer et al. *Nucl. Fusion*, 53(5):053005, 2013.

[18] L M Shao et al. *Plasma Phys. Control. Fusion*, 58(2):025004, 2016.

[19] M. Cavedon et al. *Rev. Sci. Instruments*, 88(4):043103, 2017.

[20] F. Ryter et al. *Nucl. Fusion*, 53(11):113003, 2013.

[21] G. D. Conway et al. *Phys. Rev. Lett.*, 106(6):065001, 2011.

[22] G. Birkenmeier et al. *Nucl. Fusion*, 56(8):086009, 2016.

[23] S. Potzel et al. *Nucl. Fusion*, 54(1):013001, 2013.

[24] A. Loarte et al. *Phys. Rev. Lett.*, 83:3657–3660, 18, 1999.

[25] E. Delabie et al. In *25th IAEA Fusion Energy Conference*, EX/P5–24, Austria. International Atomic Energy Agency IAEA, 2014.

[26] P.C. Stangeby. Series in Plasma Physics and Fluid Dynamics. Taylor & Francis, 2000.

[27] A. V. Chankin et al. *Nucl. Mater. Energy*, 12:273–277, 2017.

[28] C. F. Maggi et al. *Nucl. Fusion*, 54(2):023007, 2014.

[29] P.A. Schneider et al. *Nucl. Fusion*, 53(7):073039, 2013.

[30] A. M. Dimits et al. *Phys. Plasmas*, 7(3):969–983, 2000.

[31] B D Scott. *Plasma Phys. Control. Fusion*, 49(7):S25–S41, 2007.

[32] D. Told et al. *Phys. Plasmas*, 20(12):122312, 2013.

[33] N. Bonanomi et al. *Nucl. Fusion*, 59(12):126025, 2019.

[34] P. Hennequin et al. In *42nd EPS Conference on Plasma Physics*, 2015.

[35] Y. Ma et al. *Nucl. Fusion*, 52(2):023010, 2012.

[36] T Fukuda et al. *Plasma Phys. Control. Fusion*, 42(5A):A289–A297, 2000.

[37] F. Wagner. In *Workshop on Transport and Fusion Plasmas*, (Gothenburg, Sweden), 1994.

[38] J W Connor et al. *Plasma Phys. Control. Fusion*, 42(1):R1, 2000.

[39] V. Rozhansky et al. *Nucl. Fusion*, 42(9):1110–1115, 2002.

[40] V Rozhansky. *Plasma Phys. Control. Fusion*, 46(5A):A1–A17, 2004.

[41] R. Bilato et al. *to be submitted*.